Transition Metal Chemistry (2006) 31:277–285
DOI 10.1007/s11243-005-6365-4

Experimental and DFT studies on the DNA-binding properties of ruthenium(II) complexes $[Ru(phen)_2L]^{2+}$ (L = *o*-MOP, *o*-MP, *o*-CP and *o*-NP)

Wen-J. Mei and Yu-Z. Ma
School of Pharmacy, Guangdong Pharmaceutical University, Guangzhou, 510224 People's Republic of China

Jie Liu*, Jin-C. Chen, Kang-C. Zheng and Liang-N. Ji
School of Chemistry & Chemical Engineering, Sun Yat-Sen University, Guangzhou, 510275 People's Republic of China

Jun-H. Yao
Instrument Analytical & Researching Center, Sun Yat-Sen University, Guangzhou, 510275 People's Republic of China

Received 22 August 2005; accepted 20 October 2005

Abstract

A series of ruthenium(II) complexes with electron-donor or electron-acceptor groups in intercalative ligands, $[Ru(phen)_2(o\text{-MOP})]^{2+}$ (*1*), $[Ru(phen)_2(o\text{-MP})]^{2+}$ (*2*), $[Ru(phen)_2(o\text{-CP})]^{2+}$ (*3*) and $[Ru(phen)_2(o\text{-NP})]^{2+}$ (*4*), have been synthesized and characterized by elementary analysis, ES-MS, ^{1}H NMR, electronic absorption and emission spectra. The binding properties of these complexes to CT-DNA have been investigated by spectroscopy and viscosity experiments. The results showed that these complexes bind to DNA in intercalation mode and their intrinsic binding constants (K_b) are 1.1, 0.35, 0.53 and 1.7×10^5 M^{-1}, respectively. The subtle but detectable differences occurred in the DNA-binding properties of these complexes are mainly ascribed to the electron-withdrawing abilities of substituents ($-OCH_3 < -CH_3 < -Cl < -NO_2$) on the intercalative ligands as well as the intramolecular H-bond (for substituent $-OCH_3$) which increase the planarity area of the intercalative ligand to some extent. The density functional theory (DFT) calculations were also performed and used to further discuss the trend in the DNA-binding affinities of these complexes.

Introduction

For decades, much attention has been focused on the interaction of octahedral Ru(II) complexes with DNA owing to their potential utility as DNA probes, molecular light switches and chemotherapy drugs for tumors [1–8]. In general, Ru(II) complexes can bind to DNA in three non-covalent modes: intercalation, groove and electrostatic bindings. However, the binding affinity and site depend on the conformations of DNA and the structures of intercalative ligands [9–12]. Ru(II) complexes with enlarged aromatic ring, such as 2-phenylimidazo [4,5-*f*] [1,10]-phenanthroline (pip) and its substituted derivatives, can bind to DNA with strong affinity [13–18]. Furthermore, factors affecting the interactions of Ru(II) complexes with DNA have been widely studied in experiments, and the effects of planarity [19] and intramolecular hydrogen bond of intercalative ligands have been reported [20–21]. However, so far the studies on the electronic effects of Ru(II) mixed-phenanthroline complexes are still rather limited, and thus it is important and significant to carry out some discussions in this field in order to design Ru(II) complexes with better DNA-binding characteristics.

On the other hand, theoretical computations on Ru(II) complexes applying the density functional theory (DFT) method have become more and more customary [22–28], since it can describe, with reasonable accuracy, the electronic structures of systems such as transition metal complexes in which electron correlation plays an important role, and save much computational time compared with traditional *ab initio* methods [29–30]. Rillema *et al.* [31] carried out DFT calculations on Ru(II) mixed-ligands diimine complex cations to support the idea that the lowest energy transitions are metal-to-ligand charge transfer and that the LUMO is mainly located on the ligand with the lowest LUMO energy in the corresponding complex $[RuL_3]^{2+}$. Furthermore, Zhang *et al.* [32] reported hydrolysis theory for cisplatin and its analogues based on density functional studies. We recently also reported some DFT studies on the electronic structures and related properties, as well as the trend in DNA-binding for some Ru(II) polypyridyl complexes [21, 33–35]. Obviously these theoretical efforts are very significant in guiding the experimental studies.

* Author for correspondence: Tel.: +86-20-84134058; Fax: +86-20-84035497; E-mail: cesliuj@mail.sysu.edu.cn

In this paper, a series of Ru(II) complexes with electron-donor or electron-acceptor substituents in the intercalative ligands, $[Ru(phen)_2(o\text{-MOP})]^{2+}$ (*1*), $[Ru(phen)_2(o\text{-MP})]^{2+}$ (*2*), $[Ru(phen)_2$ $(o\text{-CP})]^{2+}$ (*3*) and $[Ru(phen)_2(o\text{-NP})]^{2+}$ (*4*) (Scheme 1), were synthesized and characterized. The spectroscopic and viscosity experiments were utilized to study the DNA-binding properties of these complexes, and the DFT calculations were also applied to further discuss the trend in the DNA-binding affinities.

Experimental

Chemicals

CT-DNA was purchased from the Sino-American Biotechnology Company. All reagents and solvents were purchased commercially (AR, Acros Inc. and Sigma Inc. etc.) and used without further purification unless otherwise noted. Doubly distilled water was used to prepare buffers. The concentration of calf thymus DNA was determined spectrophotomertrically using the molar absorptivity 6600 M cm^{-1} (260 nm) (The ratio of UV absorbance at 260 and 280 nm is in the range of 1.8–1.9:1).

Synthesis and characterization

$[Ru(phen)_2Cl_2]\cdot 2H_2O$ was prepared following the procedure found in the literature [36]. Ru(II) complexes (*1*), (*2*), (*3*) and (*4*) were synthesized by refluxing $Ru(phen)_2Cl_2$ and *o*-MOP (*o*-MP, *o*-CP or *o*-NP) in ethylene glycol under an Ar atmosphere in high yield. Each complex was obtained as its PF_6^- salt and was purified by column chromatography.

Electrospray mass spectrometry (ES-MS) has recently been shown to be a powerful tool for measuring the molecular mass of non-volatile and thermally unstable compounds [37]. The ES-MS for (*1*), (*2*), (*3*) and (*4*) exhibits a fragment ion peak of $(M + 1PF_6)^+$ at 933.0, 917.0, 936.9 and 947.9 (*m*/*z*), respectively (Table 1). The fragment ion peaks of M^{2+} of these complexes appear at 394.3, 386.4, 396.4 and 401.8 for (*1*), (*2*), (*3*) and (*4*), respectively, and the resolution of this peak for these complexes shows that the species is doubly charged and that the isotopic distribution corresponds to the calculated one.

The electronic absorption spectra of these Ru(II) complexes in tris-buffer are characterized by an intense ligand-centered transition in the UV region and a metal-to-ligand charge transfer transition (MLCT) in the visible region (Table 2). The lowest-energy absorption bands ascribed to the MLCT transitions for (*1*), (*2*), (*3*) and (*4*) are 455, 452, 453 and 453 nm respectively. The intense and sharp bands at 263, 263, 263 and 261 nm in UV region for (*1*), (*2*), (*3*) and (*4*), respectively, are attributed to the intraligand $\pi \rightarrow \pi^*$ transition via comparison with the spectra of $[Ru(bpy)_3]^{2+}$. Little variation in the energy of the MLCT bands with the electronic effect in intercalative ligand was observed.

Ru(II) complexes (*1*), (*2*) and (*3*) emit fluorescence in tris-buffer in the 500–700 nm range at room

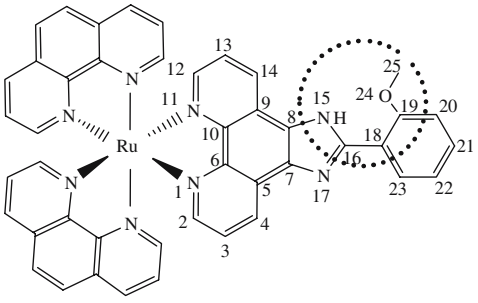

$[Ru(phen)_2(o\text{-MOP})]^{2+}$ (*1*)

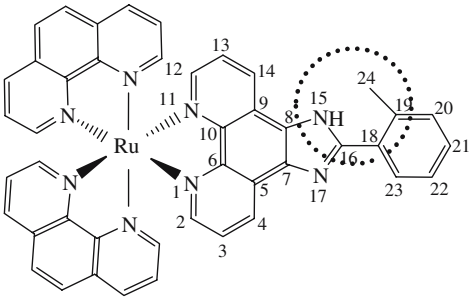

$[Ru(phen)_2(o\text{-MP})]^{2+}$ (*2*)

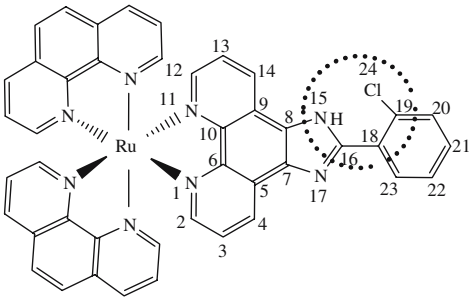

$[Ru(phen)_2(o\text{-CP})]^{2+}$ (*3*)

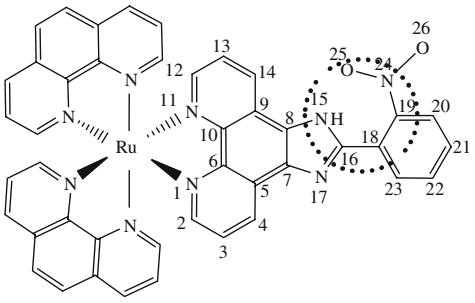

$Ru(phen)_2(o\text{-NP})]^{2+}$ (*4*)

Scheme 1. Schematic molecular structures of Ru(II) complexes.

Table 1. Data of elementary analysis and ESI-MS for Ru(II) complexes

Complex	Elementary analysis (%)			ESI-MS (m/z)	
	C	H	N		
(*1*)	47.7 (47.4)	3.11 (3.08)	10.4 (10.1)	933.0 (932.8)	394.3 (393.9)
(*2*)	48.4 (48.1)	3.12 (3.12)	10.6 (10.2)	917.0 (916.8)	386.4 (385.9)
(*3*)	46.7 (44.8)	2.74 (3.06)	10.4 (9.71)	936.9 (937.2)	396.4 (396.2)
(*4*)	45.5 (45.7)	2.81 (2.77)	11.8 (11.2)	947.9 (947.8)	401.8 (401.4)

*The calculated value is shown in bracket.

Table 2. Electronic absorption spectra and DNA-binding constants (K_b) of Ru(II) complexes

Complex	λ_0/nm	λ_b/nm	$\Delta\lambda$/nm	H%	$K_b/\times 10^5$ M^{-1}
(*1*)	455	456	1	12	1.10
	263	264	1	13	
(*2*)	452	453	1	9	0.35
	263	264	1	9	
(*3*)	453	454	1	9	0.53
	263	264	1	12	
(*4*)	453	454	1	21	1.70
	261	262	1	23	

temperature, with the maximum at 589, 588 and 589, respectively, and only a very weak fluorescence was observed for complex (*4*) under the same conditions (the maximum is at 588 nm).

2-(2-Methoxyphenyl) imidazo [4,5-f][1, 10] phenanthroline(o-MOP) (1a)

The ligand 2-(2-methoxyphenyl)imidazo[4,5-*f*][1,10] phenanthroline (*o*-MOP) was prepared by the method similar to that in [38], but with some modification.

A solution of phenanthraquinone (0.26 g, 1.2 mmol), *o*-anisaldehyde (0.24 g, 1.8 mmol) and NH_4OAc(1.9 g, 25 mmol) in 10 cm^3 glacial acetic acid was refluxed for 2 h. The cooled deep red solution was diluted with H_2O (25 cm^3), and neutralized with $NH_3 \cdot H_2O$. Then the mixture was filtered and the precipitates were washed with H_2O and Me_2CO, then dried and purified by chromatography over 60–80 mesh SiO_2 using MeOH as an eluent, yields: 0.35 g, 84%. $C_{20}H_{14}N_4O \cdot H_2O$ Calcd. (%): C: 69.7; H: 4.69; N: 16.3; Found (%): C: 69.3; H: 4.66; N: 16.2. ES-MS (in DMSO, m/z): 326.7 (calcd. 326.4).

2-(2-Methylphenyl) imidazo [4,5-f][1, 10] phenanthroline (o-MP) (2a)

o-MP was synthesized by the same method as above, but with phenanthraquinone (0.26 g, 1.2 mmol) and *o*-tolualdehyde (0.22 g, 1.8 mmole), yield: 0.31 g, 78%. $C_{20}H_{14}N_4 \cdot H_2O$ Calcd. (%): C: 73.2; H: 4.9; N: 17; Found (%): C: 73.6; H: 5.0; N: 17.4. ES-MS (in DMSO, m/z): 310.6 (calcd. 310.4).

2-(2-Chlorophenyl) imidazo [4,5-f][1, 10] phenanthroline (o-CP) (3a)

o-CP was synthesized by the same method as above, but with phenanthraquinone (0.26 g, 1.2 mmol) and 2-chlorobenzaldehyde (0.25 g, 1.8 mmole), yield: 0.32 g, 76%. $C_{19}ClH_{11}N_4 \cdot H_2O$ Calcd. (%): C: 65.4; H: 3.76; N: 16.1; Found (%): C: 65.6; H: 3.8; N: 16.4. ES-MS (in DMSO, m/z): 331.0 (calcd. 330.8).

2-(2-nitrophenyl) imidazo [4,5-f][1, 10] phenanthroline (o-NP) (4a)

o-NP was synthesized by the same method as above, but with phenanthraquinone (0.26 g, 1.2 mmol) and 2-nitrobenzaldehyde (0.27 g, 1.8 mmole), yield: 0.38 g, 87%. $C_{19}H_{11}N_5O_2 \cdot H_2O$ Calcd. (%): C: 63.5; H: 3.65 N: 19.5; Found (%): C: 63.9; H: 3.62 N: 19.1. ES-MS (in DMSO, m/z): 341.6 (calcd. 341.3).

[Ru(phen)$_2$(o-MOP)]$^{2+}$ (1)

$[Ru(phen)_2$ (*o*-MOP)$]^{2+}$ was synthesized by the method described in [39] with some modification. $[Ru(phen)_2Cl_2] \cdot 2H_2O$ (0.09 g, 0.17 mmol) and (*1a*)(0.058 g, 0.17 mmol) were added to 10 cm^3 of ethylene glycol. The mixture was then refluxed for 2 h under an Ar atmosphere. The cooled reaction mixture was diluted with H_2O (20 cm^3) and filtered to remove solid impurities. The complex was then separated from soluble impurities by precipitation with NH_4PF_6. The precipitated complex was dried, dissolved in a small amount of MeCN, and purified by chromatography over alumina oxide using MeCN-toluene (2:1, v/v) as an eluent, yield: 0.16 g, 84%. Calcd for $C_{44}F_{12}H_{30}N_8OP_2$ Ru $\cdot 2H_2O$ (%): C: 47.4; H: 3.08; N: 10.1; Found (%): C: 47.7; H: 3.11; N: 10.4; ^{1}H NMR (DMSO-d_6, δ ppm): 9.32 (1H, d); 9.08 (1H, d); 8.77 (4H, d); 8.39 (4H, s); 8.21 (2H, d); 8.14 (2H, t); 8.12 (2H, d); 8.02(2H, 2d); 7.81 (6H, m); 7.74 (1H, t); 7.35 (1H, d); 7.24 (1H, t); 4.04 (3H, s); ES-MS of the PF_6^- salt in MeCN: m/z 933.0$(M+1PF_6)^+$ (calcd: 932.8); 394.3 $(M)^{2+}$(calcd: 393.9). Absorption UV-Vis, in water at pH 7.2λ_{max}($\varepsilon/10^4$ M^{-1} cm^{-1}): 263 (8.6), 455 (1.7). No corrected emission maximum in water at pH 7.2: 589.4 nm.

[Ru(phen)$_2$ (o-MP)]$^{2+}$ (2)

[Ru(phen)$_2$(*o*-MP)]$^{2+}$ was prepared by the above-mentioned method but with (*2a*) (0.056 g, 0.17 mmol); yield: 0.14 g, 77%. $C_{44}F_{12}H_{30}N_8P_2Ru \cdot 2H_2O$ Calcd. (%): C: 48.1; H: 3.12; N: 10.2; Found (%): C: 48.4; H: 3.12; N: 10.6; ^{1}H NMR (DMSO-d$_6$, δ ppm): 9.06 (2H, d); 8.78 (4H, d); 8.39 (4H, s); 8.17 (2H, d); 8.08 (2H, d), 8.04 (2H, d); 7.85 (6H, m); 7.51 (3H, m); 7.26 (1H, t); 2.70 (3H, s); ES-MS of the PF_6^- salt in MeCN: *m/z* 917.0(M + 1PF$_6$)$^+$ (calcd: 916.8); 386.4 (M)$^{2+}$(calcd: 385.9). Absorption UV-Vis, in water at pH 7.2λ_{max} ($\varepsilon/10^4$ M^{-1} cm^{-1}): 264(9.9), 452(1.7). No corrected emission maximum in water at pH 7.2: 587.8 nm.

[Ru(phen)$_2$(o-CP)]$^{2+}$ (3)

[Ru(phen)$_2$(*o*-CP)]$^{2+}$ was prepared by the above-mentioned method but with **3a** (0.059 g; 0.17 mmol); yield: 0.15 g, 79%. $C_{43}F_{12}ClH_{27}N_8P_2Ru \cdot 4H_2O$ Calcd. (%): C: 44.8; H: 3.06; N: 9.71; Found (%): C: 44.5; H: 3.10; N: 9.81; ^{1}H NMR (DMSO-d$_6$, δ ppm): 9.03 (2H, d); 8.77 (4H, d); 8.38 (4H, s); 8.13 (2H, d); 8.07 (2H, d), 8.00 (2H, d); 7.93 (1H, d); 7.77 (6H, m); 7.64 (2H, m); 7.26 (1H, m); ES-MS of the PF_6^- salt in MeCN: *m/z* 936.9 (M + 1PF$_6$)$^+$ (calcd: 937.2); 396.4 (M)$^{2+}$(calcd: 396.2). Absorption UV-Vis, in water at pH 7.2λ_{max}($\varepsilon/10^4$ M^{-1} cm^{-1}): 263(11.6) 454(2.1). No corrected emission maximum in water at pH 7.2: 589.4 nm.

[Ru(phen)$_2$ (o-NP)]$^{2+}$ (4)

[Ru(phen)$_2$(*o*-NP)]$^{2+}$ was prepared by the above-mentioned method but with **4a** (0.061 g; 0.17 mmol); yield: 0.14 g, 74%. $C_{43}F_{12}H_{27}N_9O_2$ $P_2Ru \cdot 2H_2O$ Calcd. (%): C: 45.8; H: 2.77; N: 11.2; Found (%): C: 45.5; H: 2.81; N: 11.8; ^{1}H NMR (DMSO-d$_6$, δ ppm): 8.87 (2H, d); 8.77 (4H, d); 8.38 (4H, s); 8.21 (1H, d); 8.12 (2H, d), 8.10 (2H, d); 7.85 (2H, d); 7.76 (6H, m); 7.68 (3H, m); ES-MS of the PF_6^- salt in MeCN: *m/z* 947.9(M + 1PF$_6$)$^+$ (calcd: 947.8); 802.3 (M-H$^+$)$^+$ (calcd: 801.8); 401.8 (M) $^{2+}$ (calcd: 401.4). Resolution of the peak 401.8 shows that the species is double charged and the isotopic distribution corresponds to the calculated one. Absorption UV-Vis, in water at pH 7.2λ_{max}($\varepsilon/10^4$ M^{-1} cm^{-1}): 262(12.2) 454(2.2). No corrected emission maximum in water at pH 7.2: 588.0 nm.

Physical measurements

Microanalyses were carried out on an Elementar Vario EL elemental analyser. ES-MS were recorded on a LCQ system (Finnigan MAT, USA). The spray voltage, tube lens offset, capillary voltage and capillary temperature were set at 4.50 kV, 30.00 V, 23.00 V and 200 °C, respectively, and the quoted *m/z* values are for the major peaks due to isotope distribution. Emission spectra were measured on a Shimadzu RF-5000 spectrofluorophotometer and UV-Visble absorption was recorded on a Shimadzu UVPC-3000 spectrophotometer.

Viscosity experiments were performed on an Ulbbelodhe viscometer, immersed in a thermostatted water-bath maintained at 30.0 ± 0.1 °C. Data were presented as $(\eta/\eta_0)^{1/3}$ *versus* the concentration of [Ru]/[DNA]. Viscosity values were calculated from the observed flow time of DNA-containing solutions ($t > 100$ s) corrected for the flow time of buffer alone (t_0), i.e., $\eta = t - t_0$.

Theoretical calculations

Theorectical calculations were carried out using the G98 quantum chemistry program-package [40]. Becke's three parameters hybrid functional [25–26, 41] with the LYP correlation functional [42] (B3LYP) and an effective core potential basis set LanL2DZ [43–46] were employed in all the DFT calculations. Each of the octahedral Ru(II) complexes [Ru(phen)$_2$L]$^{2+}$ (L = *o*-MOP, *o*-MP, *o*-CP and *o*-NP) consists of Ru(II), one main ligand L or intercalative ligand, and two co-ligands (phen). There is no molecular symmetry in each of these complexes. The full geometry optimization computations and population analysis were performed for them. Based on the computational results, the schematic diagram of some frontier molecular orbital energies of [Ru(phen)$_2$L]$^{2+}$ was drawn and the structural diagrams of the complexes were also drawn with the Molden v3.7 program [47].

Results and discussion

DNA-binding properties of Ru(II) complexes

Electronic absorption spectra

In general, the complex binding to DNA in an intercalation mode exhibits a red and hypochromism shift in the absorption spectra, and the extent of spectral changes are closely correlative to the DNA-binding affinities of these complexes. The spectral shifts in an intercalation mode are usually greater than those in a groove-binding mode. In the presence of a double helix calf thymus DNA (CT-DNA), the electronic absorption spectra for all of these complexes exhibit obviously hypochromism, and the hypochromism values for (*1*), (*2*), (*3*) and (*4*) at MLCT absorption band (452–455 nm) are 12, 9, 9 and 21%, respectively (Table 2).

In order to clarify the DNA-binding affinities of these complexes, the intrinsic binding constants were calculated according to Equation (1) [48], through a plot of [DNA]/$\varepsilon_a - \varepsilon_f$ *versus* [DNA]

$$\frac{[DNA]}{\varepsilon_a - \varepsilon_f} = \frac{[DNA]}{\varepsilon_b - \varepsilon_f} + \frac{1}{K_b(\varepsilon_b - \varepsilon_f)} \quad (1)$$

where [DNA] is the concentration of DNA in base pairs, ε_a, ε_f and ε_b are respectively the apparent extinction

coefficient ($A_{obsd}/[M]$), the extinction coefficient for free metal(M) complex and the extinction coefficient for the metal(M) complex in the fully bound form. In plots of [DNA]/ $\varepsilon_a - \varepsilon_f$ *versus* [DNA], K_b is given by the ratio of slope to intercept. The calculated values for (*1*), (*2*), (*3*) and (*4*) at the MLCT absorption band are 1.1, 0.35, 0.53 and $1.7 \times 10^5\ M^{-1}$, respectively. These values are smaller than those for $[Ru(bpy)_2dppz]^{2+}$ ($> 10^6\ M^{-1}$)[49] and $[Ru(ip)_2dppz]^{2+}$ ($2.1 \times 10^7\ M^{-1}$)[50]. These data indicate that the binding affinities of these complexes to DNA increase in the sequence: (*2*) < (*3*) < (*1*) < (*4*).

Emission spectra

The interaction of the Ru(II) complexes with the double helix CT-DNA was monitored *via* luminescence. Upon the addition of CT-DNA, the emission of complex (*4*) exhibits pronounced enhancement (Figure 1), and its emission intensity increases steadily to 8.5 times relative to that of the original and reaches saturation at *ca.* [DNA]/[Ru] = 8:1. However, the emission intensities increase by 2.2, 1.7 and 1.5 for complexes (*1*), (*2*) and (*3*), respectively (Figure 2). The enhancement of emission intensities of these complexes can be attributed to the hydrophobic environment inside the DNA helix, which reduces the accessibility of water

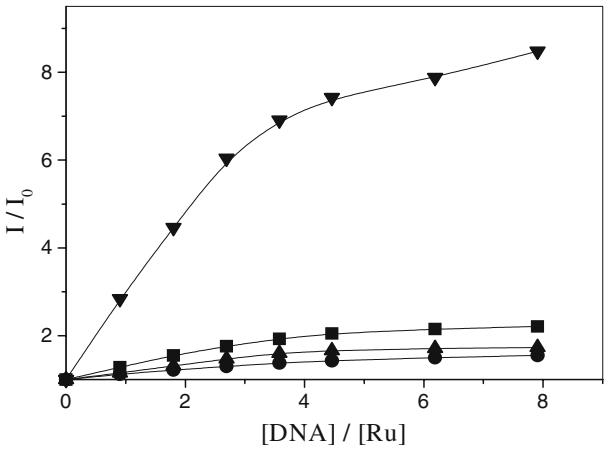

Fig. 2. Relative emission intensity (I/I_0) of Ru(II) complexes *1*(■), *2*(●), *3*(▲) and *4*(▼) in absence and in presence of increasing amount of CT-DNA.

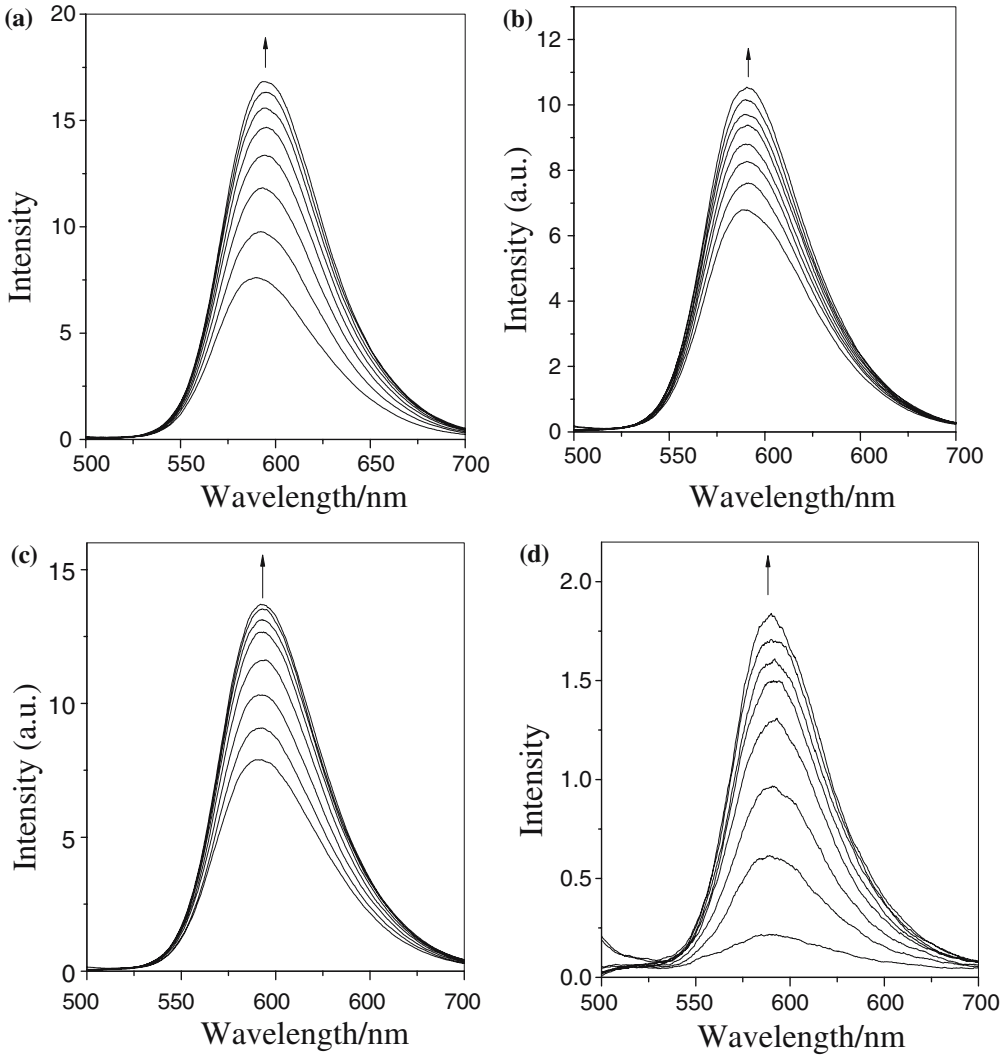

Fig. 1. Emission spectra of Ru(II) complexes *1*(a), *2*(b), *3*(c) and *4*(d) in absence and in presence of increasing amount of CT-DNA.

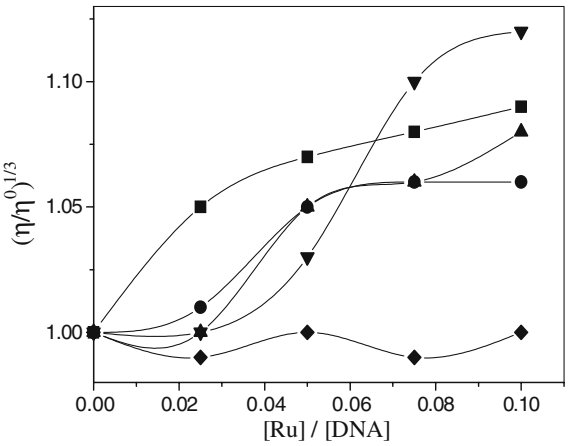

Fig. 3. Relative viscosity of CT-DNA in absence and in presence of increasing amounts of Ru(II) complexes *1*(■), *2*(●), *3*(▲), *4*(▼) and $[Ru(bpy)_3]^{2+}$ (◆) at 30 ± 0.1°C.

molecules and makes the mobility of the complexes be restricted at the binding site.

Viscosity behavior

The viscosity experiments, being sensitive to the change of length of double helix DNA, were considered as one of the most unambiguous methods to determine the binding mode of complex to DNA in absence of crystal data [51]. In general, the relative viscosity of DNA in presence of complex in an intercalation mode will be increased, because the intercalative ligand will separate the base pairs of DNA, and thus lengthen the DNA helix. On the contrary, a partial and/or non-classical intercalation of complex will reduce the relative viscosity of DNA, since the binding ligand may bend (or kink) the DNA helix and reduce its effective length [34]. The experiments on relative viscosity of rod-like CT-DNA in the presence of complexes (*1*), (*2*), (*3*) and (*4*), as well as $[Ru(bpy)_3]^{2+}$, were carried out and the results are shown in Figure 3.

The viscosity of DNA remains almost unchanged upon addition of $[Ru(bpy)_3]^{2+}$, which is consistent with an electrostatic association. However, in the presence of Ru(II) complexes (*1*), (*2*), (*3*) and (*4*) respectively, the relative viscosity of rod-like DNA was increased (Figure 3), resulting from the stacking interaction of these complexes with the base pairs of DNA and lengthens the DNA helix, indicating these complexes may bind to calf thymus DNA in a non-classical intercalation mode.

Theoretical explanation on the trend in the DNA-binding affinities of the complexes

The above experimental results showed that these Ru(II) complexes bind to DNA in intercalation mode and the DNA-binding affinities of these complexes increase in the sequence: (*2*) < (*3*) < (*1*) < (*4*). Obviously, there are subtle but detectable differences occurred in the DNA-binding properties. Such differences may be resulted from the changes of geometric and electronic structures of these complexes (especially the intercalative ligand) due to the different substituents on the intercalative ligand.

Although the single crystal structures of these Ru(II) complexes have not been obtained as far, the DFT calculations can give us some important parameters of the geometric structures of these complexes, as well as some useful information on electronic structures. The calculated geometrical structures of these complexes *via* the full geometry optimization are given in Table 3 and Figure 4. It is illustrated that the dihedral angle (N15–C16–C18–C19, shown in the dash circle in Scheme 1) closely correlates to the planarity of intercalative ligands is changed greatly though the main bond lengths and bond angles of these complexes are changed only slightly with varied substituents on the intercalative ligands. The calculated dihedral angles (N15–C16–C18–C19) of complexes (*1*), (*2*), (*3*) and (*4*) are 0.1, 25.6, 0.6 and 18.6 degree, respectively.

It is well established that there is π–π interaction between the base pairs of DNA and the intercalative ligand of metal complex in an intercalation mode. Although the whole supramolecular system formed from DNA and the complex using the DFT method can not be calculated at present for its too large in size, the complexes and the DNA model can be individually calculated by the DFT method, and the trend in the interactions between complexes and DNA can be analyzed by applying the frontier molecular orbital theory established by Fukui [52–53].

Recently, based on the investigation of energies of frontier molecular orbits, Reha and Hobza indicated that all intercalators, such as ethidium, are good electron acceptors because their LUMO energies are all negative whereas all bases and base pairs of isolated DNA, e.g., adenine, thymine, and adenine-thymine (AT), are all good electron donors and very poor electron acceptors because their LUMO energies are all positive in contrast to negative LUMO energies of

Table 3. Calculated selected bond lengths (nm) and dihedral angels (°) of $[Ru(phen)_2L]^{2+}$

Comp.	Ru–N $^{a}_{m}$	N–Ru–N $^{b}_{m}$	C–C(C–N) $^{c}_{m}$	Ru–N_{co}	N–Ru–N_{co}	C–C(C–N)$_{co}$	Dihedral angle[d]
(*1*)	0.2104	79.3	0.1405	0.2106	79.5	0.1405	−0.1
(*2*)	0.2105	79.3	0.1407	0.2106	79.4	0.1405	−25.6
(*3*)	0.2104	79.3	0.1405	0.2106	79.4	0.1405	−0.6
(*4*)	0.2104	79.3	0.1406	0.2106	79.4	0.1405	−18.6

[a]Ru–N_m: mean bond length between Ru and coordination N atoms in main ligand; Ru–N_{co}: mean bond length between Ru and coordination N atoms in co-ligand, and so on; [b]N–Ru–N_m: mean bond angle between coordination N atoms in main ligand and Ru atom, and so on; [c]C–C(C–N)$_m$ expresses the mean bond length of the intercalative ligand skeleton, and so on; [d]Dihedral angle: N15–C16–C18–C19.

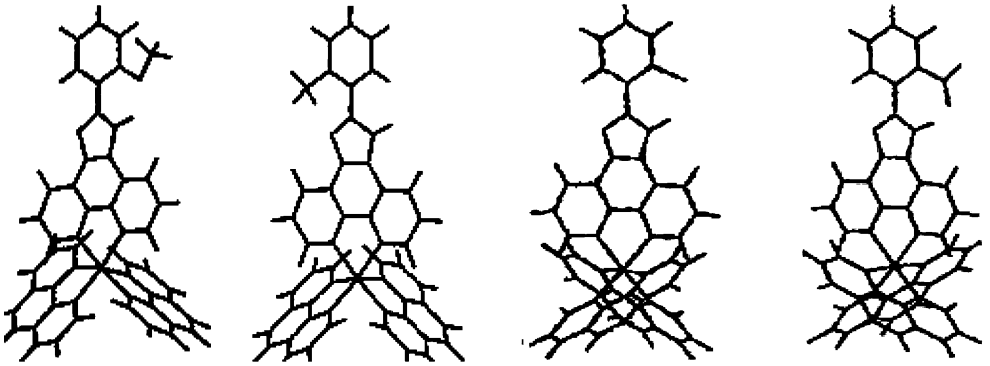

(*1*) (*2*) (*3*) (*4*)

Fig. 4. Calculated molecular structural maps of complexes $[Ru(phen)_2L]^{2+}$.

intercalator [54]. Kruita further reported the DFT results for a stacked DNA base-pair model with backbones [55]. The calculated energies of the HOMO and 6 occupied MOs lying near the HOMO for the CG/GC stacking were −1.27, −1.33, −1.69, −1.79, −1.98, −2.06 and −2.08 eV, respectively. Moreover, the components of these MOs were distributed on different sites of DNA, and the components of the HOMO and NHOMO (next HOMO) were mainly distributed on the base pairs of DNA. On the other hand, for complexes $[Ru(phen)_2L]^{2+}$(L = *o*-MOP, *o*-MP, *o*-CP and *o*-NP), the DFT results showed that the energies of their LUMOs and more than 10 unoccupied MOs lying near the LUMOs are in range of $-7.3 \sim -4.0$ eV, and the components of these MOs are predominantly distributed on the ligands, in particular, some of them are on the intercalative ligands. It can be clearly seen that the HOMO energies and occupied orbital lying near the HOMO of DNA model are all much higher than those of the LUMO and the unoccupied MOs lying near the LUMO of every one of $[Ru(phen)_2L]^{2+}$. It further suggests the studied complexes should be excellent electron acceptors in their interaction with DNA. Such a trend in the relative energies should be kept even though the orbital energies for the CG/CG stacking are replaced by those for the other base-pair stacking, because the attraction of metal complex cations with high positive charges for electrons in the frontier MOs should be much stronger than that of various DNAs.

According to the frontier molecular orbital theory, the lower LUMO energy of the complex in an intercalation mode must be advantageous to accept the electron from base pairs of DNA, and thus advantageous to the π–π interaction between the complex and DNA. Therefore, the LUMO energies of the complexes must be an important factor in correlation with their DNA-binding constants. On the other hand, the effective planarity area (*S*) of intercalative ligand of the metal complex must be another important factor, because the larger the effective planarity area (*S*) of intercalative ligand between the pairs of DNA is, the stronger the π–π stacking interaction between intercalative ligand and base pairs of DNA is, and thus the greater DNA-binding affinity of the complex is.

Some frontier molecular orbital energies, and schematic diagrams of energies of $[Ru(phen)_2L]^{2+}$ were given in Table 4, Figure 5, respectively. It is illustrated that the LUMO energies of this series of the complexes reduce in the order ε_L (*1*) > ε_L (*2*) > ε_L (*3*) > ε_L (*4*) and the energies of four unoccupied molecular orbitals lying near the LUMOs are also in such an order. If only one trend in LUMO (even including LUMO + *x*) energies is considered, the DNA-binding constants (K_b) of these complexes should be increased in the sequence: K_b (*1*) < K_b (*2*) < K_b (*3*) < K_b (*4*). However, as abovementioned, the planarity of intercalative ligand of (*1*) is all-right (the dihedral angle N15–C16–C18–C19, 0.1°) due to the intra-H-bonding between the O atom of $-OCH_3$ and the H atom of the HN(11) group in complex (*1*), which is further confirmed by the distance between the O atom of $-OCH_3$ and H atom of the HN(11) group (0.1881 nm). It is the intra-H-bonding that leads the intercalative ligand of (*1*) to increase its planar area and thus results in a stronger DNA-binding of complex (*1*) than that of (*2*) and (*3*). In addition, the binding affinity for complex (*2*) is the weakest, and this can be attributed to its higher LUMO energy and rather non-planarity intercalative ligand (the dihedral angle N15–C16–C18–C19,

Table 4. Some frontier molecular orbital energies (ε_i/a.u.) of the complexes

Comp.	H−1	HOMO[a]	LUMO[b]	L + 1	L + 2	L + 3	L + 4
(*1*)	−0.3783	−0.3616	−0.2643	−0.2610	−0.2578	−0.2562	−0.2552
(*2*)	−0.3806	−0.3697	−0.2679	−0.2644	−0.2613	−0.2610	−0.2591
(*3*)	−0.3936	−0.3800	−0.2680	−0.2646	−0.2617	−0.2611	−0.2593
(*4*)	−0.3941	−0.3886	−0.2684	−0.2648	−0.2644	−0.2614	−0.2608

[a]HOMO (or H): the highest occupied molecular orbital; [b]LUMO (or L): the lowest unoccupied molecular orbital.

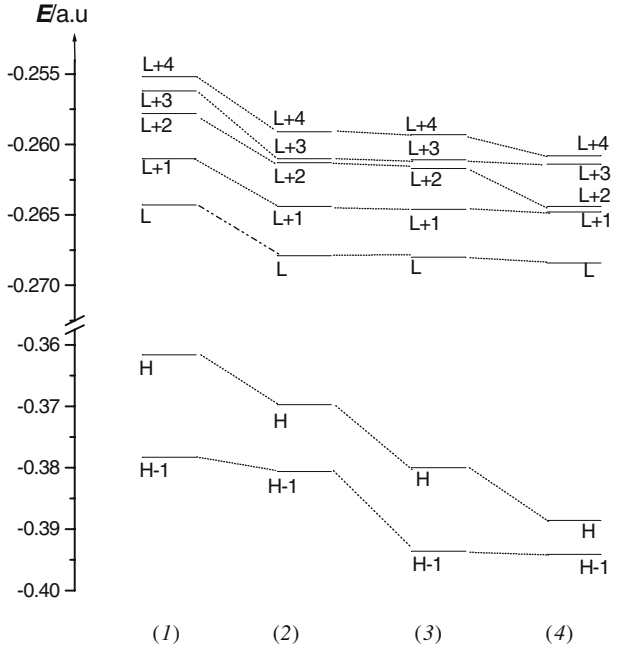

Fig. 5. Schematic diagram of some frontier MO energies of $[Ru(phen)_2L]^{2+}$ (H: HOMO; H-1: HOMO-1; L: LUMO; L + *x*: LUMO + *x*.)

25.6°). As for complex (*4*), since its LUMO and (LUMO + *x*) energies are the lowest correspondingly in this series, and there is also intramolecular H-binding between H(HN) and O(–NO_2) (Figure4) leading the effective planarity area (*S*) of intercalative ligand to increase to compensate the non-planarity effect (the dihedral angle N15–C16–C18–C19, 18.6°) between phenyl and imidazo[4,5-*f*][1, 10] phenanthroline in the intercalative ligand. It is the reason why the DNA-binding constant K_b (*4*) is the greatest in this series. Therefore, synthetically considering both the LUMO energy and effective planarity area (*S*) of these complexes, the trend in the DNA-binding constants K_b (*2*) < K_b (*3*) < K_b (*1*) < K_b (*4*) can be reasonably explained.

Conclusions

A series of Ru(II) complexes with electron-donor or electron-acceptor groups in intercalative ligands, $[Ru(phen)_2(o\text{-MOP})]^{2+}$(*1*), $[Ru(phen)_2(o\text{-MP})]^{2+}$(*2*), $[Ru(phen)_2(o\text{-CP})]^{2+}$(*3*) and $[Ru(phen)_2(o\text{-NP})]^{2+}$(*4*) were experimentally confirmed to bind to DNA in intercalation mode, and their intrinsic DNA-binding constants(K_b) were measured to be 1.1, 0.35, 0.53 and $1.7 \times 10^5\ M^{-1}$, respectively. These data showed that there were subtle but detectable differences occurred in the DNA-binding properties of these Ru(II) complexes and that such differences can be mainly attributed to the electron-withdrawing abilities of the substituents (–OCH_3 < –CH_3 < –Cl < –NO_2) on the intercalative ligands of these complexes. In addition, the intramolecular H-bond (for substituent –OCH_3) also plays a role to some extent because it leads the increase of planarity area of the intercalative ligand. The DFT calculations were also performed and used to further discuss the trend in the DNA-binding affinities for these Ru(II) complexes.

Acknowledgements

We are grateful to the National Nature Science Foundation of China, the Nature Science Foundation of Guangdong Province, the Nature Science Foundation for Doctoral Initial of Guangdong Province, the Item of Tackle Key Problem of Science and Technology of Guangzhou City, the Medicine Science and Technology Foundation of Guangdong Province for their financial support.

References

1. M.J. Clarke, *Coord. Chem. Rev.*, **236**, 209 (2003).
2. C.-W. Jiang, H. Chao, H. Li and L.-N. Ji, *J. Inorg. Biochem.*, **93**, 247 (2003).
3. H.C.M. Yau, H.L. Chan and M. Yang, *Sensor. Actuat. B: Chem.*, **81**, 283 (2002).
4. K.K. Patel, E.A. Plummer, M. Darwish, A. Rodger and M.J. Hannon, *J. Inorg. Biochem.*, **91**, 220 (2002).
5. Y.N.V. Gopal, N. Konuru and A.K. Kondapi, *Arch. Biochem. Biophys.*, **401**, 53 (2002).
6. M. Bouma, B. Nuijen, M.T. Jansen, G. Sava, A. Bult and J.H. Beijnen, *J. Pharm. Biomed. Anal.*, **30**, 1287 (2002).
7. O. Nováková, C. Hofr and V. Brabec, *Biochem. Pharmacol.*, **60**, 1761 (2000).
8. L. Mishra, A.K. Yadaw, S. Srivastava and A.B. Patel, *New J. Chem.*, **24**, 505 (2000).
9. W. Chen, C. Turro, L.A. Friedman, J.K. Barton and N.J. Turro, *J. Phys. Chem. B*, **101**, 6995 (1997).
10. R.C. Lasey, S.S. Banerji and M.Y. Ogawa, *Inorg. Chim. Acta*, **300–302**, 822 (2000).

11. C. Moucheron, A.K.-D. Mesmaeker and J.M. Kelly, *J. Photochem. Photobiol. B: biol.*, **40**, 91 (1997).
12. J.G. Goll and H.H. Thorp, *Inorg. Chim. Acta*, **242**, 219 (1996).
13. C.G. Coates, P. Callaghan, J.J. McGarvey, J.M. Kelly, L. Jacquet and A.K.-D. Mesmaeker, *J. Mol. Struct.*, **598**, 15 (2001).
14. M.J. Clarke, *Coord. Chem. Rev.*, **232**, 69 (2002).
15. L.-N. Ji, X.-H. Zou and J.-G. Liu, *Coordin. Chem. Rev.*, **216–217**, 513 (2001).
16. H. Chao, W.-J. Mei, Q.-W. Huang and L.-N. Ji, *J. Inorg. Biochem.*, **92**, 165 (2002).
17. K.E. Erkkila, D.T. Odom and J.K. Barton, *Chem. Rev.*, **99**, 2777 (1999).
18. C.J. Murphy and J.K. Barton, *Method. Enzymol.*, **226**, 576 (1993).
19. Q.-X. Zhen, B.-H. Ye, Q.-L. Zhang, J.-G. Liu, H. Li, L.-N. Ji and L. Wang, *J. Inorg. Biochem.*, **76**, 47 (1999).
20. J.-G. Liu, B.-H. Ye, H. Li, Q.-X. Zhen, L.-N. Ji and Y.-H. Fu, *J. Inorg. Biochem.*, **76**, 265 (1999).
21. W.-J. Mei, J. Liu, K.-C. Zheng, L.-J. Lin, H. Chao, A.-X. Li, F.-C. Yun and L.-N. Ji, *Dalton Trans.*, 1352 (2003).
22. M. Stener and M. Calligaris, *J. Mol. Struct. Theochem.*, **497**, 91 (2000).
23. D.P. Chong, *Recent Advances in Density Functional Methods*, World Scientific, Singapore, 1995.
24. M. Calligaris and N.S. Panina, *J. Mol. Struct.*, **646**, 61 (2003).
25. P. Hohenberg and W. Kohn, *Phys. Rev. B*, **136**, 864 (1964).
26. A.D. Becke, *J. Chem. Phys.*, **98**, 1372 (1993).
27. A. Gorling, *Phys. Rev. A*, **54**, 3912 (1996).
28. Q. Wang, Y.-J. Ye, F. Chen and H. Zhao, *Biophys. Chem.*, **75**, 129 (1998).
29. T. Ziegler, V. Tschinke, J.K. Labanowsky and J.W. Andzelm, *Density Functional Methods in Chemistry*, Springer, New York, 1991.
30. K. Naing, M. Takahashi, M. Taniguchi and A. Yamagishi, *Inorg. Chem.*, **34**, 350 (1995).
31. S.R. Stoyanov, J.M. Villegas and D.P. Rillema, *Inorg. Chem.*, **41**, 2941 (2002).
32. Y. Zhang, Z.J. Guo and X.Z. You, *J. Chem. Soc.*, **123**, 9378 (2001).
33. K.-C. Zheng, J.-P. Wang, W.-L. Peng, X.-W. Liu and F.-C. Yun, *J. Phys. Chem. A*, **105**, 10899 (2001).
34. K.-C. Zheng, J.-P. Wang, Y. Shen, W.-L. Peng and F.-C. Yun, *Dalton Trans.*, 111 (2002).
35. K.-C. Zheng, X.-W. Liu, J.-P. Wang, F.-C. Yun and L.-N. Ji, *J. Mol. Struct. Theochem.*, **637**, 195 (2003).
36. B.P. Sullivan, D.J. Salmon and T.J. Meyer, *Inorg. Chem.*, **17**, 3334 (1978).
37. R. Arakawa, S. Tachiyashiki and T. Matsuo, *Anal. Chem.*, **67**, 4133 (1995).
38. E.A. Steck and A.R. Day, *J. Am. Chem. Soc.*, **65**, 452 (1943).
39. R. Hage, J.G. Haasnoot, J. Reedijk, R. Wang, E.M. Ryan, J.G. Vos, A.L. Spek and A.J.M. Duisenberg, *Inorg. Chim. Acta*, **174**, 77 (1990).
40. R.P. Hertzberg and P.B. Dervan, *J. Am. Chem. Soc.*, **104**, 313 (1982).
41. M.J. Frisch, G.W. Trucks, H.B. Schlegel, G.E. Scuseria, M.A. Robb, J.R. Cheeseman, V.G. Zakrzewski, J.A. Montgomery Jr., R.E. Stratmann, J.C. Burant, S. Dapprich, J.M. Millam, A.D. Daniels, K.N. Kudin, M.C. Strain, O. Farkas, J. Tomasi, V. Barone, M. Cossi, R. Cammi, B. Mennucci, C. Pomelli, C. Adamo, S. Clifford, J. Ochterski, G.A. Petersson, P.Y. Ayala, Q. Cui, K. Morokuma, N. Rega, P. Salvador, J.J. Dannenberg, D.K. Malick, A.D. Rabuck, K. Raghavachari, J.B. Foresman, J. Cioslowski, J.V. Ortiz, A.G. Baboul, B.B. Stefanov, G. Liu, A. Liashenko, P. Piskorz, I. Komaromi, R. Gomperts, R.L. Martin, D.J. Fox, T. Keith, M.A. Al-Laham, C.Y. Peng, A. Nanayakkara, M. Challacombe, P.M.W. Gill, B. Johnson, W. Chen, M.W. Wong, J.L. Andres, C. Gonzalez, M. Head-Gordon, E.S. Replogle and J.A. Pople, *Gaussian 98*, Gaussian Inc., Pittsburgh PA, 2002 Revision A.11.4.
42. A.D. Becke, *J. Chem. Phys.*, **98**, 5648 (1993).
43. C. Lee, W. Yang and R.G. Parr, *Phys. Rev. B*, **37**, 785 (1988).
44. P.J. Hay and W.R. Wadt, *J. Chem. Phys.*, **82**, 270 (1985).
45. W.R. Wadt and P.J. Hay, *J. Chem. Phys.*, **82**, 284 (1985).
46. J.B. Foresman and A.E. Frisch, *Exploring Chemistry with Electronic Structure Methods*, 2nd edn. Gaussian Inc., Pittsburgh, PA, 1996.
47. G. Schaftenaar and J.H. Noordik, *J. Comput.-Aided Mol. Design*, **14**, 123 (2000).
48. A. Wolfe, G.H. Shimer and T. Meehan, *Biochemistry*, **26**, 6392 (1998).
49. S. Satyanarayana, J.C. Dabrowiak and J.B. Chaires, *Biochemistry*, **32**, 2573 (1993).
50. J.-G. Liu, B.-H. Ye, H. Li, L.-N. Ji, R.-H. Li and J.-Y. Zhou, *J. Inorg. Biochem.*, **73**, 2081 (1999).
51. S. Satyanarayana, J.C. Dabrowiak and J.B. Chaires, *Biochemistry*, **31**, 9319 (1992).
52. K. Fukui, T. Yonezawa and H. Shingu, *J. Chem. Phys.*, **20**, 722 (1952).
53. I. Fleming, *Frontier Orbital and Organic Chemical Reaction*, Wiley, New York, 1976.
54. D. Reha, M. Kabelac, F. Ryjacek, J. Sponer, J.E. Sponer, M. Elstner, S. Suhai and P. Hobza, *J. Am. Chem. Soc.*, **124**, 3366 (2002).
55. N. Kurita and K. Kobayashi, *Comput. Chem.*, **24**, 351 (2000).